



OPEN Photophysiologicaly active green, red, and brown macroalgae living in the Arctic Polar Night

Natalie Summers^{1✉}, Glauca M. Fragoso¹ & Geir Johnsen^{1,2}

Arctic macroalgae species have developed different growth strategies to survive extreme seasonal changes in irradiance in polar regions. We compared photophysiological parameters such as the light saturation parameter (E_k) and pigment composition of green, red, and brown macroalgae collected in January (Polar Night) and October 2020 (end of the light season). Macroalgae in January appeared healthier (morphologically) and had longer lamina (new growth) than those in October. E_k values for red, and brown algae were higher with lower maximum quantum yield of PS II fluorescence (F_v/F_m) in January versus October. Furthermore, in January, new tissues in kelp species had higher E_k than the older tissue. Higher E_k and lower F_v/F_m during the Polar Night indicates that the photosynthetic apparatus is active but slow. Furthermore, we discuss Chlorophyll (Chl) a emission spectra under blue and green excitation light to determine the ratio of Chl a in photosystem II (PS II) vs photosystem I (PS I). Absorbance spectra of *P. palmata* was used to interpret the emission spectra. The observed spectral shifts in the absorbance and reflectance spectra of different macroalgae is discussed. Photophysiological methods provide health information complementary to future mapping and monitoring of macroalgae. These results reveal that macroalgae grow new tissue in darkness.

Macroalgae are important primary producers of coastal ecosystems, providing substrate, food, and shelter for organisms of different trophic levels^{1,2}. Primary production in macroalgae is primarily controlled by irradiance (E) in the spectral range of 400 to 700 nm (E_{PAR}), but other key environmental variables, such as temperature and nutrient availability also modulate the rate of photosynthesis^{3–6}. In Svalbard (longitude of 79°N), the winter solstice on December 22nd marks the darkest day of the Polar Night, with December and January being the two darkest months with monthly average E_{PAR} of 67 E^{-06} $\mu\text{mol photons m}^{-2} \text{s}^{-1}$ in December 2019 and 234 E^{-06} $\mu\text{mol photons m}^{-2} \text{s}^{-1}$ in January 2020. On the other hand, the monthly average E_{PAR} during the summer solstice in June 2020 was 392 $\mu\text{mol photons m}^{-2} \text{s}^{-1}$ when measured from the “ArcLight” observatory located about 4 km west of Ny-Ålesund (78.9°N, 11.9°E)⁷. Despite the extreme E values, some Arctic macroalgae have been reported to grow in low light conditions and tolerate darkness for longer periods (up to 18 months)⁸. For instance, a study conducted in October 2016 and February 2017 on the eco-physiology of *Laminaria solidungula*, an endemic Arctic brown macroalgae species, and *Saccharina latissima*, a boreal species, suggested that kelp species can maintain their photosynthetic capabilities during the Polar Night^{2,9}. *Laminaria solidungula* can store energy gained from photosynthesis to grow during the winter darkness^{9–12}. *Saccharina latissima* can delay its growth period until the late spring/summer when light is available^{2,13,14}. Growth and survival of these macroalgal species during the Polar Night rely, known so far, on the usage of stored sugar compounds accumulated through photosynthesis during previous summers^{8,9}. While it has been shown that many polar organisms (e.g. zooplankton and fish) are highly sensitive to small changes in light intensity during the Polar Night^{15,16}, little is known about the photobiological responses of macroalgae during this period of extreme darkness.

Photophysiological responses of macroalgae are not only related to light quantity (intensity of E) but also quality (spectral irradiance $E(\lambda)$). For example, the kelp forest canopy limits light penetration with a decrease in light intensity and spectral composition (mostly green light available) for species living below, partly resulting in the zonation of macroalgae^{8,17,18}. Understanding the underwater light climate (E_{PAR} , $E(\lambda)$), and photoperiod) is thus crucial for studies on photosynthesis. Irradiance and the corresponding color ($E(\lambda)$) available are important factors for light utilization in photosynthesis¹⁹. During photosynthesis, excitation energy is either absorbed and utilized by light harvesting pigments, dissipated as fluorescence by chlorophyll a (Chl a) or dissipated as heat²⁰. Different pigment composition in macroalgae determines their classification into green, brown, and red

¹Centre for Autonomous Marine Operations and Systems (AMOS), Trondheim Biological Station, Department of Biology, Norwegian University of Science and Technology (NTNU), Trondheim, Norway. ²University Centre in Svalbard (UNIS), Longyearbyen, Norway. ✉email: natalie.summers@ntnu.no

algae as well as which wavelengths they can absorb and utilize²¹. The pigment concentrations also affect the ability of macroalgae to harvest light of different wavelengths and is thus linked to their photosynthetic ability. Each macroalgal light harvesting pigment has different *in-vivo* light absorption characteristics with chlorophylls absorbing in blue (400–500 nm) and red (600–700 nm), carotenoids absorbing mostly in 400–530 nm range and phycobiliproteins absorbing in the blue–green to green range at 500–570 nm². Studying spectral light utilization of algae can explain how they pre-condition their photosynthetic apparatus before light increasingly and rapidly becomes available in late winter/spring²².

Increasing temperatures, sedimentation rates and decreasing sea ice cover over the past decade in Kongsfjorden, Svalbard, have altered the underwater light climate, such as darkening of the fjord in summer^{23,24} and resulted in changes in the vertical distributions of algae species^{2,18}. This highlights the need for more studies on health state, and seasonality of macroalgae. Enabling technologies have led to more efficient ways of *in-situ* monitoring and mapping of kelp forests. In 2004 hyperspectral imaging (HI) from an airplane was used to map and identify the kelp forest in Ny-Ålesund during the light season²⁵. More recently, in January 2020, mapping of the kelp forest in Ny-Ålesund was conducted during the Polar Night using underwater hyperspectral imager (UHI) carried by a novel miniature remotely operated vehicle (ROV) system²⁶. This study is the first to carry out photobiological and health state assessment of the most common species of green, brown, and red macroalgae during the Polar Night simultaneously with *in-situ* identification and mapping of the biodiversity and areal cover of the same kelp forest using a UHI from an ROV²⁶.

In this study, we measured and compared photosynthetic parameters (photosynthetic efficiency α , maximum relative electron transport rate, $rETR_{max}$, the onset light saturation parameter, E_K , and maximum quantum yield of PS II fluorescence, F_v/F_m) of the most common species of green, red, and brown macroalgae from Kongsfjorden during the Polar Night (January) and at the end of the polar light season (October 2020). These measurements were paired with pigment composition of each of the experimental species as well as the *in vivo* PS II-Chl a emission spectra under green (525 nm) and blue (452 nm) excitation light, using a spectrometer attached to the Diving PAM II. The primary aim of this study was to determine the photophysiological state of old versus new tissues of different macroalgae species to elucidate seasonal differences. Additionally, we provided a first attempt to interpret emission spectra under blue and green excitation light to infer pigment activity and distribution in the photosystems. Finally, we discuss how the photophysiology of macroalgae affect the absorbance and reflectance spectra and how this can be integrated into future habitat mapping using *in-situ* spectral reflectance per image pixel from mini-ROV with UHI.

Methods and materials

Study site and conditions

Macroalgal specimens were sampled between 1 and 3 m depth, 50 m off the coast of the Marine Laboratory in Ny-Ålesund located in Kongsfjorden, Svalbard (78°55′40.0″N 11°55′52.9″E, Fig. 1). Other specimens were also collected on the 11th of January 2020, as part of the Polar Night cruise aboard research vessel Helmer Hanssen,



Figure 1. Map showing our study area in Kongsfjorden, Svalbard (78°55′40.0″N 11°55′52.9″E). Localization of our macroalgae sampling site (green diamond) next to the UHI transect (red line) from Summers et al.²⁶ and located in front of the marine lab (black square) in Ny-Ålesund. Location of aerial hyperspectral imaging study sites from Volent et al.²⁵ are shown as blue dots marked 4 and 5. Base map from <https://toposvalbard.npolar.no/>, courtesy of the Norwegian Polar Institute.

and on the 26th of October 2020 during a research stay in Ny-Ålesund. The bay in front of the Marine Laboratory was between 0.5 to 4 m deep and characterized with rocky and sandy substrate covered with macroalgae. In the shallow areas (closest to shore) ice formed on the beach (ice foot) and corresponding free moving sea ice had caused ice scouring of macroalgae in the upper 1.5 m due to tidal range of approximately 1.3 m (no visible macroalgae). Above water surface irradiances were provided by the ArcLight observatory located about 4 km west of Ny-Ålesund (78.9°N, 11.9°E) and using an all-sky camera as irradiance sensor. Specifications of the different light measuring instruments and calibration procedure, as well as data from 2017–2020 were published by Johnsen et al.⁷. Samples from the 11th of January 2020 was part of the Polar Night season with E_{PAR} far below the theoretical threshold to induce actinic activity. The average E_{PAR} above the water surface for January 2020 was $234 \text{ E}^{-06} \mu\text{mol photons m}^{-2} \text{ s}^{-1}$ versus a theoretical irradiance to induce photosynthesis set at $0.01 \mu\text{mol photons m}^{-2} \text{ s}^{-1}$. The weather was calm and water temperature was at -1.8°C resulting in the formation of pancake ice on the surface of the bay. The average downwelling E_{PAR} above the water surface in October 2020 was $6.6 \mu\text{mol photons m}^{-2} \text{ s}^{-1}$. However, October is also a light transition period when light availability decreases throughout the month with only 44% of hours per month being above E_{PAR} of $0.01 \mu\text{mol photons m}^{-2} \text{ s}^{-1}$, inducing photosynthetic activity. On the 26th of October 2020 (day of sample collection), the weather was calm with clear seawater at a temperature of 1.5 to 2°C .

In January 2020, we collected 3 specimens of each of the 5 species of macroalgae by snorkeling; the green alga (Chlorophyceae) *Ulva* sp., the red alga (Rhodophyceae) *Palmaria palmata*, and the brown algae (Phaeophyceae), consisting of the kelp species *Laminaria digitata* (morphologically similar to *Saccharina nigripes*, synonym to *Hedophyllum nigripes*, see the discussion^{18,27}), *Alaria esculenta*, and *Saccharina latissima*. The algal specimens were collected during two sampling sessions, 12 h apart, during which the experimental specimens were kept in collection nets at the collection site and 1 m depth. Once back onboard the research vessel Helmer Hanssen, the living specimens were stored in a dark cooling room (4°C) in buckets full of freezing seawater, providing an *in-situ* temperature of -1.8°C , until experiments were carried out at the same temperature²⁶. Specimens were kept in the dark at all times until experiments were conducted. Specimen collection in January 2020 was conducted at the same time as an ROV-based survey using underwater hyperspectral imaging (UHI) [results published in 26]. The UHI-based mapping provided information on biodiversity and abundance of the different macroalgae groups as described by Summers et al.²⁶, with the present study providing additional information on the photophysiological state of the species.

In October, we collected 3 specimens of each experimental species of macroalgae (*Ulva* sp., *P. palmata*, *L. digitata*, *A. esculenta*, and *S. latissima*) that were kept in an outdoor aquarium with running seawater in the same light and temperature conditions as *in-situ* ($+1.5$ to 2°C , average E_{PAR} of $6.6 \mu\text{mol m}^{-2} \text{ s}^{-1}$ measured by the light observatory in October 2020⁷). For each specimen of *Ulva* sp. in January and in October, a subsample of 2–5 cm^2 of tissue was cut out. For *P. palmata*, tissue subsamples were taken from the base (old tissue) and from the apex of the lamina (new growth). For the 3 kelp species, *A. esculenta*, *L. digitata*, and *S. latissima*, subsamples were taken from the meristem where new tissue forms on the lamina, and from the apex, which represents the oldest tissue that can be 3–4 years old (Fig. 2)²⁸.

Statistical test

For each subsample collected in January and October (tissue samples from *Ulva* sp., new and old tissue of kelp species) we conducted rapid light curves, Chl a emission spectra and HPLC pigments, giving us triplicate data for each experimental species. One-way ANOVA test was conducted on the data from *Ulva* sp. to see whether there were any significant differences in the E_K , F_v/F_m , and pigment concentrations between seasons. Two-way ANOVA was conducted on the data from the red and brown algae to test for significant differences in the E_K , F_v/F_m , and pigment concentrations between seasons and between tissue age. We report the F-value (representing the variation between sample means versus the variation within the samples) and the *p*-value that determines whether differences between group means are statistically significant. We consider $p < 0.05$ as significant. A post hoc Tukey's test was conducted to find which variables differed.

Rapid light curves (RLC)

Rapid light curves (RLC) measure photosynthetic performance of PS II versus irradiance in a similar way to traditional photosynthetic vs irradiance curves (P vs E) but with shorter light incubation periods (here we used 30 s) at each irradiance²⁹. As a result, steady state conditions of photosynthesis are not achieved in the RLC and the maximum PS II fluorescence quantum yield ($\phi_{\text{PSII}}^{\text{max}}$ —more commonly written as F_v/F_m , see Eq. 1) and relative transport rate (rETR) reflect the actual state of photosynthesis (not the optimal state shown by a P vs E curve). RLC reflects the short-term acclimation from the past few minutes but is also influenced by the long-term (weeks to months) acclimation pre-history of algae²⁹.

We used the underwater Chl a Fluorometer Diving PAM II from Walz (Effeltrich, Germany) with the Win-Control-3 Software (Heinz Walz GmbH, Effeltrich, Germany) for our RLC measurements. All measurements were done either on fully charged battery (9V) or connected to a power supply (12 V). The Diving PAM II uses a red LED with an emission peak of 654 nm as a measuring light source, which we set to E_{PAR} of $0.19 \mu\text{mol photons m}^{-2} \text{ s}^{-1}$ for most samples to avoid triggering photosynthetic activity. Samples were exposed to red stepwise increasing E_{PAR} for actinic illumination from 0 to $446 \mu\text{mol photons m}^{-2} \text{ s}^{-1}$ in 12 steps (0, 7, 14, 20, 27, 38, 56, 85, 125, 186, 243, 341, and $445 \mu\text{mol photons m}^{-2} \text{ s}^{-1}$), with 30 s incubation time. The Diving PAM II detected Chl a fluorescence from PS II using a PIN photodiode protected by long-pass and short-pass filters, thus measuring the 730 nm Chl a emission shoulder (termed chl a fluorescence) at 12-bit resolution (dynamic range).

The macroalgae tissue was secured in the magnetic sample holder that was attached to an optical fiber at one end, and the Diving PAM II on the other end. The sample holder was placed in seawater bath without algal tissue

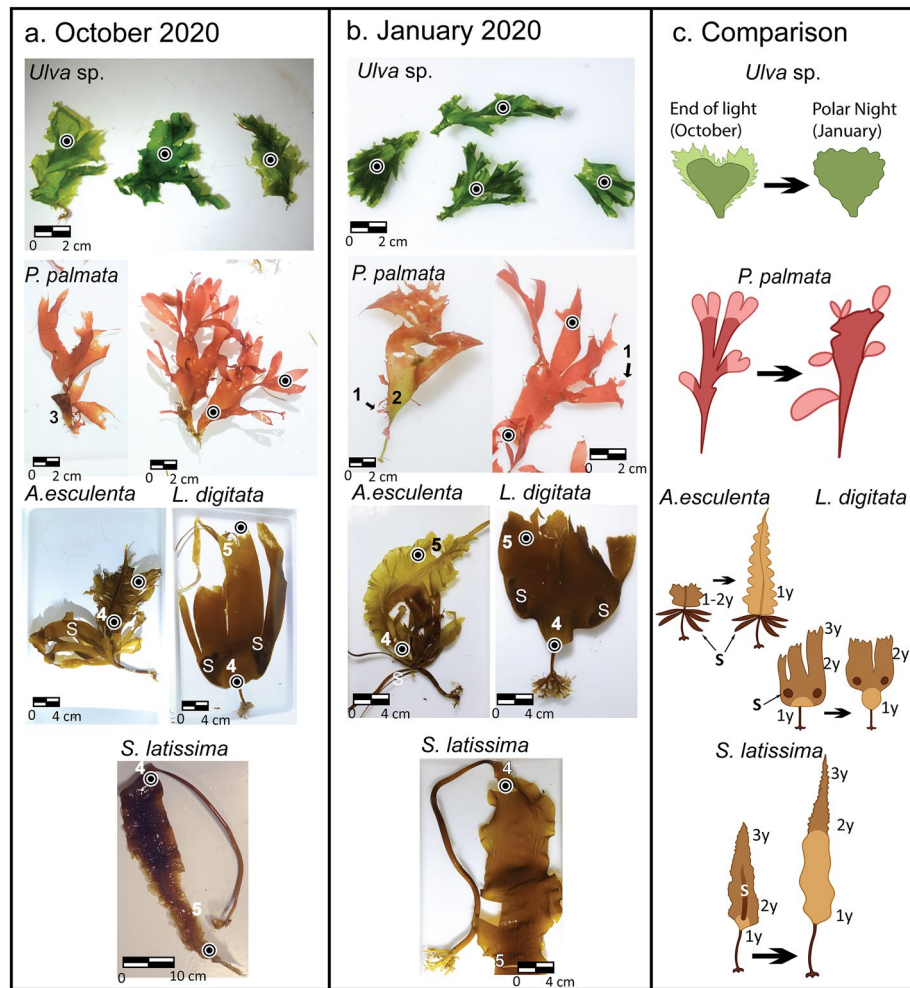


Figure 2. Macroalgal species collected in October (a) and January (b) 2020 from Kongsfjorden, Svalbard. Black dots show where tissue samples were taken for RLC, *in-vivo* Chl *a* emission spectra and pigment analysis. The green algae *Ulva* sp. had dark and non-degraded tissue on the edge of the lamina in January, while in October the tissue was pale green and degraded on the edges of the lamina. *Palmaria palmata* had new tissue growing on the edges of the thallus in January (1) often with a greenish thallus base (2), indicating old tissue with a loss of phycoerythrin (2). In October, the main thallus of *P. palmata* was growing from the thallus of the previous year (3). In the three kelp species, the growth zones are located at the meristem (4) while the older tissue is at the apex of the lamina (5). The sori (S) are also clearly visible for *A. esculenta*, and *L. digitata* in both January and October. (c) Sketches show the cycle from the end of the light season in October (left image) to the Polar Night (January, right image) with new tissue in lighter color compared to old tissue (darker). For brown algae, (1y, 2y, 3y) denotes age (in years) of the tissue. The lamina of *S. latissima* during the Polar Night was 40 to 90 cm long. Illustrations in (c) by Malin Bø Nevstad.

at *in-situ* temperature and salinity (-1.8°C in January and $+1.5^{\circ}\text{C}$ in October) to provide an autozero of Chl *a* fluorescence prior to measurements on tissues. Once the algal tissue sample was placed in the sample holder, we checked that the fluorescence emission was between 200 and 600 mV at 730 nm to ensure a good signal-to-noise ratio at all irradiances provided. The online fluorescence emission (F_t) was between 200–600 mV and the shape of the fluorescence induction curve was checked to ensure that the minimum fluorescence (F_0) and the maximum fluorescence (F_m) were stable before starting the RLC³⁰.

We measured the F_0 and F_m after dark acclimation for at least 5 min^{30,31} when approximately all functional reaction centers are open (oxidized state). These also represent the first measurement of the RLC (when E_{PAR} of actinic light = 0). The maximum quantum yield of PS II fluorescence, F_v/F_m , was then calculated on dark acclimated chloroplast following Eq. 1^{20,30}.

$$\phi_{\text{PSII}}^{\text{max}} = F_v/F_m = (F_m - F_0)/F_m \quad (1)$$

For each E_{PAR} incubation step, we measured the minimum fluorescence in actinic light (F), and the maximum fluorescence level (F'_m). The operational PS II fluorescence quantum yield in actinic light (ϕ'_{PSII}) was calculated using the Eq. (2)²⁰

$$\phi'_{PSII} = (F_m' - F)/F_m' \quad (2)$$

The relative electron transport rate (rETR) is a measure of the photosynthetic rate was calculated from ϕ'_{PSII} and E_{PAR} (3).

$$rETR = \phi'_{PSII} * E_{PAR} \quad (3)$$

The RLC data was curve fitted to rETR to find photosynthetic-irradiance parameters based on the Webb et al. (1974) model with the R software v. 3.4.3³² using the Phytotools package with the Nelder-Mead fit method Eq. 4^{33,34}. We obtained the photosynthetic efficiency (α) from the linear part of the RLC and the maximum relative electron transfer rate $rETR_{max}$ (indicating P_{max} , maximum photosynthetic rate) to calculate the light saturation parameter, E_K ($\mu\text{mol photons m}^{-2} \text{s}^{-1}$) Eq. 4–5,^{19,30}.

$$rETR = \alpha * E_K * (1 * e^{E_{PAR}/E_K}) \quad (4)$$

$$E_K = rETR_{max}/\alpha \quad (5)$$

***In-vivo* Chl a emission spectra from PS II**

The *in-vivo* Chl a emission spectra under blue and green excitation light show PS II emission peaks at 685 and 730 nm. Blue and green excitation light are absorbed and funneled by light harvesting pigments to Chl a in PS II^{17,35,36}. The resulting emission of Chl a fluorescence indicates light energy transfer from light harvesting complexes (LHC II) bonded to in the highly fluorescent PS II (95% of *in vivo* fluorescence) vs PS I (< 5% of fluorescence)^{37–39}. Comparing the relative emission intensities under the different light excitations may help elucidate the relative amount of Chl a bonded to PS II vs PS I.

The algal samples were positioned between a magnetic dark chamber tissue holder and disk (40 mm diameter, 10 mm height) padded with foam rubber. We then used the mini spectrometer on the Diving PAM II, which consists of a polyoxymethylene tube (35 mm diameter, 13 mm height) with blue and green LED excitation bands (light rod). The blue excitation light has a peak at 452 nm, and intensity was set to 200 relative units and green excitation light (peak at 525 nm) intensity set to 600 relative units for each measurement. The spectrometer has an emission spectral range of 400–850 nm with a spectral resolution of 8–10 nm⁴⁰. Each emission spectra were measured in the range 600–850 nm using the auto-range setting that automatically determines the optimal integration time (both excitation and emission). The different integration times are subsequently considered when calculating the units of the light emission in $\text{nmol photons m}^{-2} \text{s}^{-1}$ ⁴⁰.

HPLC (high-performance liquid chromatography) isolated light-harvesting pigments

After measurements with Diving PAM II, excess water was wiped off each algal tissue sample, wrapped in aluminum foil and preserved in -80°C freezer onboard the ship and in the laboratory at the Trondheim Biological Station (TBS) at NTNU, respectively, for further analysis. Samples were kept frozen in dry ice during transport. Each sample was lightly dabbed with paper tissue to remove excess water and then weighed (wet weight). We extracted the chlorophylls and carotenoids in 5 mL of 100% methanol for 4 h in the dark at 4°C (total pigment extraction). We then filtered the pigment extract using a disposable syringe with a 2 μm filter in a 2 mL HPLC vial. The extracts were run through HPLC system from Hewlett Packard 1100 Series, following method described by^{41,42}. This HPLC uses an HP 1100 autosampler, HP 1100 series quaternary pump, HP 1100 series thermostatic column compartment and an HP 1100 series diode array detector. The eluent system uses methanol for rinsing, a solution of methanol, acetonitrile, and aquation pyridine (50:25:25) and a solution of acetone and acetonitrile (20:80). Pigments were then detected at 440nm.

***In-vivo* absorbance spectra**

For *P. palmata*, we conducted an additional experiment in May 2022 from the same field site in Kongsfjorden to measure the total *in-vivo* absorbance (dimensionless) of *P. palmata* (all LHC's and PS's) and the corresponding fraction of light absorbed by PS II (consisting of LHC II and PS II), denoted a_{PSII} ^{30,39,43}. This is an approach to estimate the fraction of light absorbed by PS I vs PS II enabling us to interpret and verify results from the *in-vivo* Chl a emission spectra. LHC II of the red algae *P. palmata* comprising water soluble phycobiliproteins, dominated by phycoerythrin (PE), bonded to PS II only^{21,43}. Since *P. palmata* also has the majority of Chl a bonded to non-fluorescent PSI^{21,39,43} we used data from this species to interpret the *in-vivo* Chl a emission spectra data described in section above.

New growth tissue (apex) of three specimens of *P. palmata* specimens were used. We measured the spectral absorbance of whole tissue and isolated the water soluble fraction of LHC II and PS II between 400 to 800 nm (1 nm spectral resolution, $n = 3$, see description in next paragraph). We used a QE Pro spectrometer (Ocean Insight Inc., Orlando, FL, USA) equipped with a 1 cm cuvette fitted into an Ocean Insight cuvette holder. The light-leading optical fiber (Ocean Optics QP1000-2-VIS-BX VIS/NIR) was pointing at the cuvette at one end and a corresponding optical fiber (Ocean Optics QP1000-2-VIS-BX VIS/NIR, 2 m long and 1 mm in fiber diameter) measured the absorbance on the other end of the cuvette in a dark room. The light source was an HL-2000-HP high-power tungsten halogen light source from Ocean Insight Inc. (Ocean Insight Inc., Orlando, FL, USA).

We used filtered seawater (with no algae sample) as a blank. For the total *in-vivo* absorbance spectra, a section of the lamina was put into a 1×1 cm (4 mL) quartz cuvette with 1 cm optical path length. The tissue was pressed vertically onto the detector side of the cuvette, with the detection sensor directed at the light source (transmittance/absorbance set up) and with an integration time of 100 ms. After measurement of the tissue, the sample

was taken out of the cuvette and grinded with a porcelain mortar and pestle with ca. 20 ml filtered seawater (0.1 μm filter) at *in-situ* temperature (used as a buffer and extractant [21, 43]). The mortar and pestle were used for 10 min to extract the water-soluble light-harvesting pigments, i.e., the phycobiliproteins dominated by PE (LHC II and PS II) found in *P. palmata*⁴³. The pigment protein extract was then filtered using a 10 mL syringe with 0.4 μm polycarbonate filter and transferred to a quartz cuvette for spectral absorbance measurements. The filtered solution, free of light-scattering particles, was pink and clear (no scattered light detected).

The absorbance spectra were scaled to an absorbance of 0 at 800 nm (light scattering correction). After this, the spectra were normalized so that the PE peaks at 495 and 545 nm of LHC II and PS II spectra matched the corresponding peaks of the *in vivo* absorption spectra. A match at 495 nm indicates that 100% of the phycobiliproteins (LHC II) are bonded to PS II^{39,43}. The difference spectra between the total absorbance curve and the fraction of light absorbed by a_{PSII} represents the non-fluorescent fraction of LHC I and PS I was done in accordance with Johnsen and Sakshaug³⁷.

In-vivo reflectance spectra

Spectral reflectance is essential for mapping method that involve hyperspectral imaging and can be used to study biodiversity and biomass of macroalgae [examples 25, 26]. The reflectance spectra are determined by pigment-specific bio-optical properties of algae.

Reflectance measurement of green (*Ulva* sp.), red (*P. palmata*), and brown algae (*A. esculenta*, *L. digitata*, and *S. latissima*) were conducted in January (described in Summers et al. 2020²⁵) using the QE Pro spectrometer with the same type of light source and fibers as described above. The same method was used in May to measure reflectance on the green algae *Ulva* sp., the red algae *P. palmata* and the brown algae *S. latissima*. For reflectance measurements, the light source and detection fiber were at a 45° angle from the algal tissue.

Results

Morphology

Macroalgal specimens collected in January 2020 were, in general, in better health condition indicated by visual inspections than the same species collected in October 2020 (Fig. 2). In the case of *Ulva* sp. (Chlorophyte), specimens were visually darker green in January and with no partial degradation at the edges of the lamina compared to the specimens collected in October. In January, the new tissue of *P. palmata* (Rhodophyte) was growing at the apex of the lamina and around the edges of the old part of the lamina. In contrast, in October, the new tissue was growing at the apex of the lamina. The lamina of the brown algal (Phaeophytes) kelp species (*A. esculenta*, *L. digitata* and *S. latissima*) were characterized by 3-year-old tissue at the apex of the lamina, 2-year-old tissue in the mid-section and tissue of 1-year-old or less at the meristem (new growth, Fig. 2). Fertile tissue (sorus) could be detected on all kelp species in both seasons except for *S. latissima* in January. The 2- and 3-year-old part of the lamina of the kelp species showed signs of deterioration. In the cases of the *A. esculenta* and *S. latissima*, the lamina was shorter (reduced and partly degenerated) in October compared to January.

Rapid light curves (RLC)

Overall, the photosynthetic parameters differed significantly between seasons in all species. The E_K was significantly different between January and October for red and brown algae. There were also significant differences between new tissue and old tissue in January as detailed below. (Fig. 3, Table 1).

For the green algae *Ulva* sp., F_v/F_m was significantly lower in January versus October ($F = 11.63$, $p > 0.01$). α and $rETR_{\text{max}}$ were both significantly higher in January than in October ($F = 149.2$, $p < 0.001$ for α and $F = 11.78$, $p < 0.01$ for $rETR_{\text{max}}$). However, E_K did not change significantly ($p > 0.05$) between seasons.

For the red algae, *P. palmata*, F_v/F_m differed significantly between seasons ($F = 7.71$, $p < 0.01$) with F_v/F_m being lower in new tissue in January versus new tissue in October (Tukey post-poc test). There was not a significant difference of the photosynthetic parameters between old and new tissue (α of 0.25–0.30 and $rETR_{\text{max}}$ of ~ 15 giving E_K of ~ 50 $\mu\text{mol photons m}^{-2} \text{s}^{-1}$, Fig. 3). However, there was a significant difference in the E_K between seasons ($F = 20.289$, $p < 0.001$ with higher E_K in new tissue in January compared to both new and old tissue in October (Tukey post-hoc test).

In the case of the kelp species, seasons significantly affected F_v/F_m as well as E_K in all 3 species, and tissue age was significant factor for E_K in *L. digitata* and *S. latissima*. New tissue of *A. esculenta*, *L. digitata* and *S. latissima* had lower F_v/F_m in January than in October ($F = 9.01$, $p < 0.01$, $F = 39.373$, $p < 0.001$, $F = 4.954$, $p < 0.05$ respectively). For *S. latissima*, F_v/F_m was also significantly lower in new tissue compared to old tissue for both January and October. E_K in new tissues in January were generally two times higher E_K (100–200 $\mu\text{mol photons m}^{-2} \text{s}^{-1}$) than the old tissues in January ($E_K \sim 50 \mu\text{mol photons m}^{-2} \text{s}^{-1}$). In contrast, in October, there was no significant difference of the photosynthetic parameters between old and new tissues (α of 0.25 and $rETR_{\text{max}} < 15$ resulting in $E_K < 50 \mu\text{mol photons m}^{-2} \text{s}^{-1}$). Specifically, for *A. esculenta*, E_K was significantly different between seasons ($F = 12.106$, $p < 0.001$) with the Tukey post-hoc test showing that E_K was higher in new tissue in January compared to new and old tissue in October. For *L. digitata*, E_K differed significantly between seasons ($F = 48.873$, $p < 0.001$) and between tissue age ($F = 5.605$, $p < 0.01$). E_K of both new tissue and old tissue from January were higher than new and old tissue from October, respectively. In addition, during the Polar Night, E_K was higher in new tissue than in old tissue. Similarly, E_K in *S. latissima* was significantly different between seasons ($F = 59.33$, $p < 0.001$) and between tissue age ($F = 32.05$, $p < 0.001$). E_K for new tissue was higher in January than in October. In addition, E_K in January was higher in new tissue compared to old tissue.

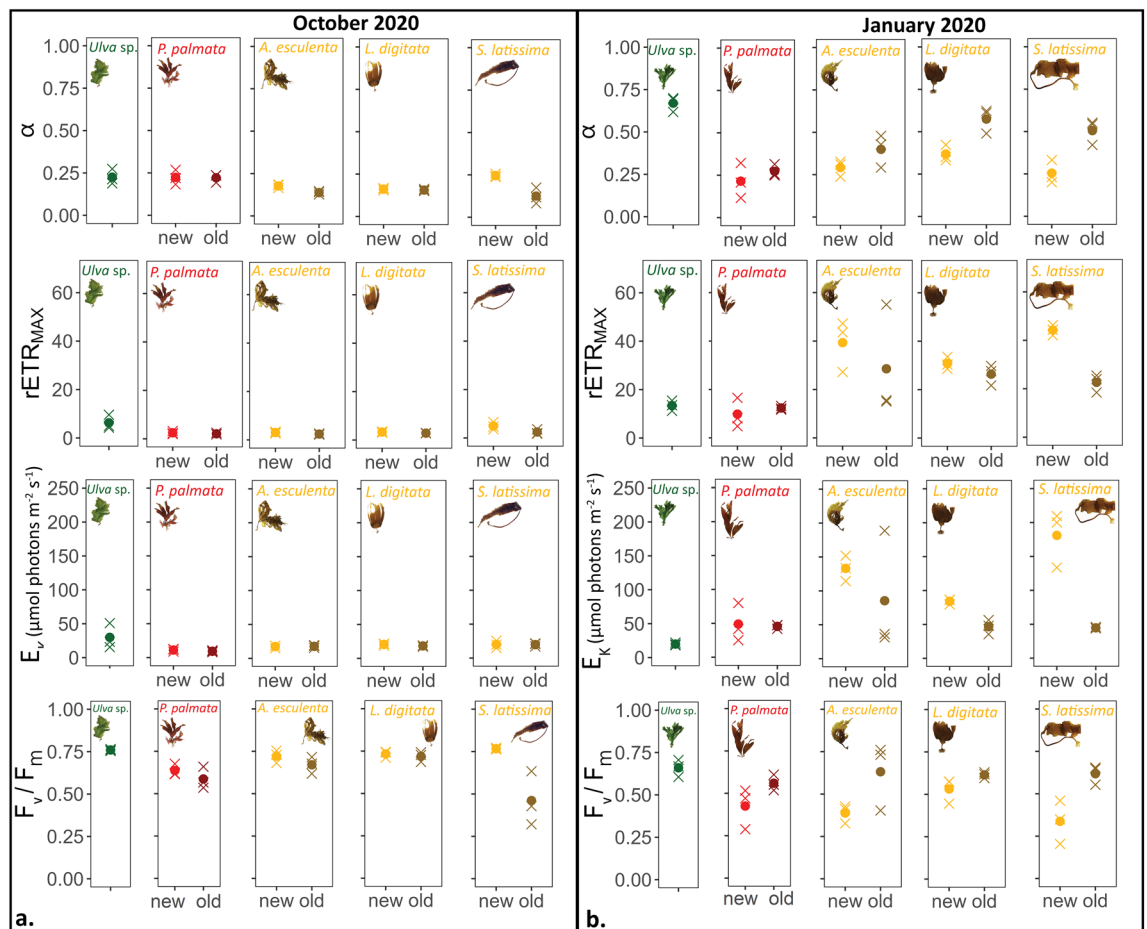


Figure 3. Photosynthetic parameters in green, red, and brown macroalgae, comprising photosynthetic efficiency (a), maximum relative electron transport rate ($rETR_{MAX}$), light saturation parameter (E_K), and the maximum quantum yield in the dark (F_v/F_m) derived from RLC measured in (a) October and (b) January. The mean values are represented by dots and the individual measurements ($n = 3$) are represented by crosses. For statistical significance see RLC section in results.

Pigments

Figure 4 shows the differences in pigment concentrations between January and October as well as between new and old tissue with the results of the Anova tests in Table 2. Chlorophyll a was the dominant pigment in all species (Fig. 4). In *Ulva* sp., concentration of light harvesting pigments per wet weight were significantly higher (at least twice as high) in January compared to in October for all major pigments. Chlorophyll a was $\sim 2500 \mu\text{g Chl a g ww}^{-1}$ in January compared to $\sim 1000 \mu\text{g Chl a g ww}^{-1}$ in October ($F = 47.19, p < 0.001$), chlorophyll b (Chl b) concentrations were $\sim 1000 \mu\text{g Chl b g ww}^{-1}$ in January vs $\sim 400 \mu\text{g Chl b g ww}^{-1}$ in October ($F = 62.4, p < 0.001$), Lutein (Lut) were $\sim 350 \mu\text{g Lut g ww}^{-1}$ in January vs $\sim 150 \mu\text{g Lut g ww}^{-1}$ in October ($F = 38.26, p < 0.001$), followed by neoxanthin (neo) and violaxanthin (viola) with ~ 80 and $\sim 112 \mu\text{g pigment g ww}^{-1}$ respectively in January and ~ 40 and $\sim 50 \mu\text{g pigment g ww}^{-1}$ respectively in October ($F = 27.04, p < 0.001$ for neo and $F = 28.04, p < 0.001$ for viola). Additionally, $\beta\epsilon$ carotene ($\beta\epsilon$ car) was found only in October ($\sim 50 \mu\text{g } \beta\epsilon\text{-car g ww}^{-1}$).

In new tissue of *P. palmata* there was significant difference in Chl a concentrations for tissue age ($F = 17.553, p < 0.001$) with $2 \times$ higher concentrations of Chl a in new tissue in January ($\sim 350 \mu\text{g Chl a g ww}^{-1}$) than in new tissue in October ($\sim 150 \mu\text{g Chl a g ww}^{-1}$) and old tissue from January ($\sim 45 \mu\text{g Chl a g ww}^{-1}$). Lutein concentrations per wet weight followed a similar trend with significant differences over seasons ($F = 5.689, p < 0.01$) and tissue age ($F = 29.003, p < 0.001$). Lutein was found in higher concentration in new tissue in January ($\sim 75 \mu\text{g Lut g ww}^{-1}$) compared to new tissue in October ($\sim 30 \mu\text{g Lut g ww}^{-1}$) and old tissue in January ($\sim 10 \mu\text{g Lut g ww}^{-1}$). $\beta\beta$ carotene ($\beta\beta$ car) and $\beta\epsilon$ carotene ($\beta\epsilon$ car) were found only in the new tissue in January ($\sim 4 \mu\text{g pigment g ww}^{-1}$ and $\sim 20 \mu\text{g pigment g ww}^{-1}$ respectively). $\beta\beta$ carotene was found in both new and old tissue in October (~ 10 and $\sim 5 \mu\text{g } \beta\beta\text{-car g ww}^{-1}$ respectively).

Concentration of pigments per wet weight in brown algae were highest in *A. esculenta*, followed by *L. digitata* and *S. latissima*. Only slight differences (but not significant, $p > 0.05$) in pigment concentrations were observed between January and October, whereas there were some stronger differences (but not significant, $p > 0.05$) in pigment concentration between new and old tissue. *Alaria esculenta* had similar Chl a concentration in both new and old tissue at $\sim 750 \mu\text{g Chl a g ww}^{-1}$ in January and $820\text{--}860 \mu\text{g Chl a g ww}^{-1}$ in October. *L. digitata* had 175 and $300 \mu\text{g Chl a g ww}^{-1}$ in new and old tissue respectively in January compared to 160 and $275 \mu\text{g Chl a g ww}^{-1}$ in October.

Species	Effects	PS II parameters	F value	p
<i>Ulva</i> sp.	Seasons	α	149.2	$p < 0.001$
		$rETR_{max}$	11.78	$p < 0.01$
		E_k	0.858	$p > 0.05$
		F_v/F_m	11.63	$p < 0.01$
<i>P. palmata</i>	Seasons	α	0.39	$p > 0.05$
		$rETR_{max}$	24.66	$p < 0.001$
		E_k	20.289	$p < 0.001$
		F_v/F_m	7.71	$p < 0.01$
	Tissue age	α	0.65	$p > 0.05$
		$rETR_{max}$	0.36	$p > 0.05$
		E_k	0.10	$p > 0.05$
		F_v/F_m	0.98	$p > 0.05$
<i>A. esculenta</i>	Seasons	α	36.12	$p < 0.001$
		$rETR_{max}$	18.21	$p < 0.001$
		E_k	12.11	$p < 0.001$
		F_v/F_m	9.01	$p < 0.01$
	Tissue age	α	1.19	$p > 0.05$
		$rETR_{max}$	0.61	$p > 0.05$
		E_k	0.81	$p > 0.05$
		F_v/F_m	2.42	$p > 0.05$
<i>L. digitata</i>	Seasons	α	150.00	$p < 0.001$
		$rETR_{max}$	328.29	$p < 0.001$
		E_k	193.49	$p < 0.001$
		F_v/F_m	39.37	$p < 0.001$
	Tissue age	α	15.39	$p < 0.001$
		$rETR_{max}$	3.03	$p > 0.05$
		E_k	36.00	$p < 0.001$
		F_v/F_m	2.01	$p > 0.05$
<i>S. latissima</i>	Seasons	α	36.65	$p < 0.001$
		$rETR_{max}$	491.81	$p < 0.001$
		E_k	59.33	$p < 0.001$
		F_v/F_m	4.95	$p < 0.05$
	Tissue age	α	4.07	$p > 0.05$
		$rETR_{max}$	80.69	$p < 0.001$
		E_k	32.05	$p < 0.001$
		F_v/F_m	0.04	$p > 0.05$

Table 1. ANOVA comparing the effects of seasons and tissue age on the photosynthetic parameters in green, red, and brown algae. Significant values ($p < 0.05$) are shown in bold.

ww^{-1} in new and old tissue in October. *Saccharina latissima* had ~ 130 and $300 \mu\text{g Chl a g } ww^{-1}$ in new and old tissue respectively in January compared to 340 and $162 \mu\text{g Chl a g } ww^{-1}$ in new and old tissue in October. In most of the brown algae older tissue had slightly more Chl a than the new tissue by a factor of 1.5 to 2, except for *A. esculenta* that was similar in both seasons, and *S. latissima*, where new tissue had 2 times more Chl a than old tissue in October.

Concentrations of Chl c ($\text{Chl } c_1 + c_2$), which is a characteristic pigment in brown algae, were similar between seasons, with variations in concentrations between new and old tissue in some species. *Alaria esculenta* had similar concentrations of Chl c across all measurements with ~ 120 – $140 \mu\text{g Chl c g } ww^{-1}$. *Laminaria digitata* had higher concentrations of Chl c in old tissue with $50 \mu\text{g Chl c g } ww^{-1}$ compared to new tissue ($30 \mu\text{g Chl c g } ww^{-1}$) in both seasons. In contrast, *S. latissima*, in January, had lower pigment concentration in the old tissue with $\sim 23 \mu\text{g Chl c g } ww^{-1}$ compared to new tissue $\sim 45 \mu\text{g Chl c g } ww^{-1}$. However, the reverse was seen in *S. latissima* in October with new tissue having higher concentrations of Chl c ($\sim 60 \mu\text{g Chl c g } ww^{-1}$) compared to old tissue ($\sim 30 \mu\text{g Chl c g } ww^{-1}$).

Fucoxanthin (fuco) was the second most abundant light harvesting pigment in the brown algae species. Fucoxanthin was found in slightly lower concentrations in *A. esculenta* in January compared to October (~ 195 – $205 \mu\text{g fuco g } ww^{-1}$ in January vs ~ 240 – $250 \mu\text{g fuco g } ww^{-1}$ in October). Similarly, *L. digitata* had lower concentrations of fuco in new tissue ($\sim 60 \mu\text{g fuco g } ww^{-1}$ in both seasons) compared to old tissue (~ 85 – $95 \mu\text{g fuco g } ww^{-1}$). Concentrations of fuco in *S. latissima* was lower in the new tissue in January ($\sim 30 \mu\text{g fuco g } ww^{-1}$) compared to old tissue in January ($\sim 75 \mu\text{g fuco g } ww^{-1}$). However, in October, new tissue had higher concentrations of fuco

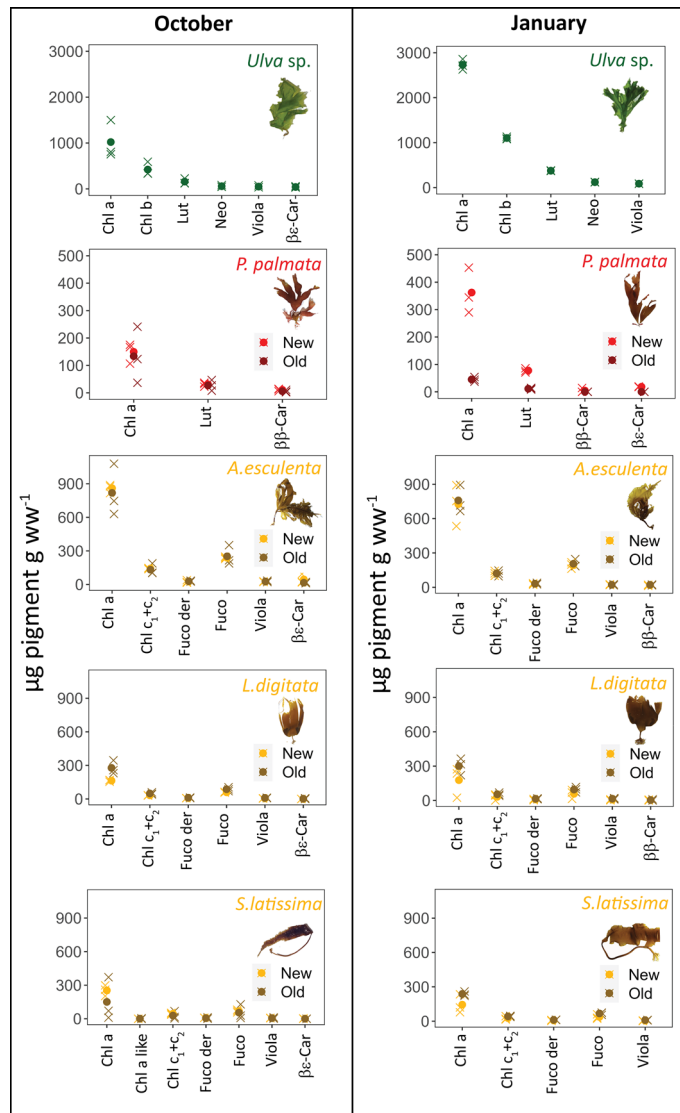


Figure 4. Pigment concentrations ($\mu\text{g pigment g ww}^{-1}$) in green, red, and brown macroalgae in new tissue (left box in light brown or red) and old tissue (right box in dark brown or red), as well as between seasons (left: October, right: January). The mean values are represented by dots and the individual measurements ($n = 3$) are represented by crosses. Pigment nomenclature from⁴² with pigment abbreviations as follows: Chl a = chlorophyll a, Chl b = chlorophyll b, Lut = lutein, Neo = neoxanthin, Viola = violaxanthin $\beta\epsilon$ -Car = $\beta\epsilon$ carotene, $\beta\beta$ -Car = $\beta\beta$ carotene, Chl $c_1 + c_2$ = chlorophyll c_1 and c_2 , Fuco = fucoxanthin, Fuco der = fucoxanthin derivative. For statistical significance see Pigments section in results.

($\sim 100 \mu\text{g fuco g ww}^{-1}$) compared to older tissue ($\sim 60 \mu\text{g fuco g ww}^{-1}$). Violaxanthin were found in lower concentrations but followed a similar trend to the other pigments in the brown algae. *Alaria esculenta* had ~ 22 and $\sim 25 \mu\text{g viola g ww}^{-1}$ in January and October respectively with no difference between new and old tissue ($p > 0.05$). Similarly, old tissue of *L. digitata* had $2 \times$ the viola concentration of the old tissue in both seasons ($\sim 5 \mu\text{g viola g ww}^{-1}$ in new tissue vs ~ 10 – $15 \mu\text{g viola g ww}^{-1}$ in old tissue). Whereas, in January, new tissue of *S. latissima* had a concentration of $5 \mu\text{g viola g ww}^{-1}$ compared to $\sim 5 \mu\text{g viola g ww}^{-1}$ in old tissue. In October, the new tissue of *S. latissima* had $10 \mu\text{g viola g ww}^{-1}$ compared to old tissue which had $\sim 5 \mu\text{g viola g ww}^{-1}$. Finally, in January, in *S. latissima*, we found $\beta\beta$ car with concentrations of ~ 3 – $11 \mu\text{g } \beta\beta \text{ car g ww}^{-1}$. In contrast, in October we found $\beta\epsilon$ car with concentrations of 3 – $45 \mu\text{g } \beta\epsilon \text{ car g ww}^{-1}$.

***In-vivo* Chl a emission spectra from PS II under blue and green excitation light**

The *in-vivo* Chl a emission spectra represent the fluorescence emission of Chl a from PS II characterized by an emission peak at 685 nm and a corresponding shoulder at 730 nm (Fig. 5). Most emission spectra had the same shape except for January spectra of *P. palmata* that had no peak at 685 and a reduced shoulder at 730 under blue excitation light. However, the emission intensity varied between species and seasons.

Species	Effects	Pigments	F value	<i>p</i>
<i>Ulva</i> sp.	Seasons	Chl a	47.19	<i>p</i> < 0.001
		Chl b	62.4	<i>p</i> < 0.001
		Lut	38.26	<i>p</i> < 0.001
		Neo	27.04	<i>p</i> < 0.001
		Viola	28.04	<i>p</i> < 0.001
<i>P. palmata</i>	Seasons	Chl a	2.45	<i>p</i> > 0.05
		Lut	5.69	<i>p</i> < 0.01
		ββ-Car	4.18	<i>p</i> > 0.05
	Tissue age	Chl a	17.55	<i>p</i> < 0.001
		Lut	59.00	<i>p</i> < 0.001
		ββ-Car	2.71	<i>p</i> > 0.05
<i>A. esculenta</i>	Seasons	Chl a	1.10	<i>p</i> > 0.05
		Chl c	0.91	<i>p</i> > 0.05
		Fuco	2.60	<i>p</i> > 0.05
		Viola	1.82	<i>p</i> > 0.05
	Tissue age	Chl a	0.003	<i>p</i> > 0.05
		Chl c	0.10	<i>p</i> > 0.05
		Fuco	0.20	<i>p</i> > 0.05
		Viola	0.24	<i>p</i> > 0.05
<i>L. digitata</i>	Seasons	Chl a	1.01	<i>p</i> > 0.05
		Chl c	0.05	<i>p</i> > 0.05
		Fuco	0.06	<i>p</i> > 0.05
		Viola	2.35	<i>p</i> > 0.05
	Tissue age	Chl a	0.003	<i>p</i> > 0.05
		Chl c	4.18	<i>p</i> > 0.05
		Fuco	5.22	<i>p</i> > 0.05
		Viola	9.65	<i>p</i> < 0.01
<i>S. latissima</i>	Seasons	Chl a	0.03	<i>p</i> > 0.05
		Chl c	0.06	<i>p</i> > 0.05
		Fuco	0.22	<i>p</i> > 0.05
		Viola	0.03	<i>p</i> > 0.05
	Tissue age	Chl a	0.01	<i>p</i> > 0.05
		Chl c	0.003	<i>p</i> > 0.05
		Fuco	0.16	<i>p</i> > 0.05
		Viola	1.46	<i>p</i> > 0.05

Table 2. ANOVA comparing the effects of seasons and tissue age on the pigment concentrations in green, red, and brown algae. Significant values ($p < 0.05$) are shown in bold.

For October samples, the Chl a fluorescence emission spectra followed a similar trend as the January emission spectra for all experimental species. However, the emission intensity was $\sim 4 \times$ higher in October compared to January in *Ulva* sp. and *P. palmata* and $\sim 2 \times$ higher for the kelp species.

In *Ulva* sp., Chl a fluorescence emission was slightly higher under green excitation light relative to tissue exposed to blue excitation light (fluorescence emission mean of ~ 600 vs ~ 400 nmol $m^{-2} s^{-1}$ in January and ~ 3000 vs ~ 2500 nmol photons $m^{-2} s^{-1}$ in October). In contrast, *P. palmata*, Chl a emission was $\sim 10 \times$ higher when exposed to green excitation light relative to blue excitation light (fluorescence emission mean of ~ 750 vs ~ 75 nmol photons $m^{-2} s^{-1}$ in January, ~ 4000 vs ~ 500 nmol photons $m^{-2} s^{-1}$ in October). In addition, there was more variability in the new tissue than in the older tissue. Similarly, in brown algae, Chl a emission was $\sim 2 \times$ higher under green excitation light.

***In-vivo* absorbance and reflectance spectra**

The *in-vivo* absorbance curves of *P. palmata* (Fig. 6a) show PE peaks at 540 nm and 570 nm for the total absorbance and the corresponding fraction of light absorbed by a_{PSII} . The *in-vivo* Chl a absorbance red peak was at 679 nm for the total absorption of *P. palmata* and at 676 nm for fraction of light absorbed by a_{PSII} . The Chl a peak in the non-fluorescent fraction of LHC I and PS I was at 681 nm. We, thus, observed a shift of 5 nm in the Chl a absorbance peak between the fluorescent (LHC II and PS II) and non-fluorescent (LHCI and PSI) spectra. In addition, the Chl a peak of fraction of light absorbed by a_{PSII} was 40% of the total absorption.

The *in-vivo* emission spectra of *P. palmata* under blue and green excitation light measured in May (Fig. 6b) was similar to the emission spectra of the same species measured in October (Fig. 5) characterized by an *in-vivo*

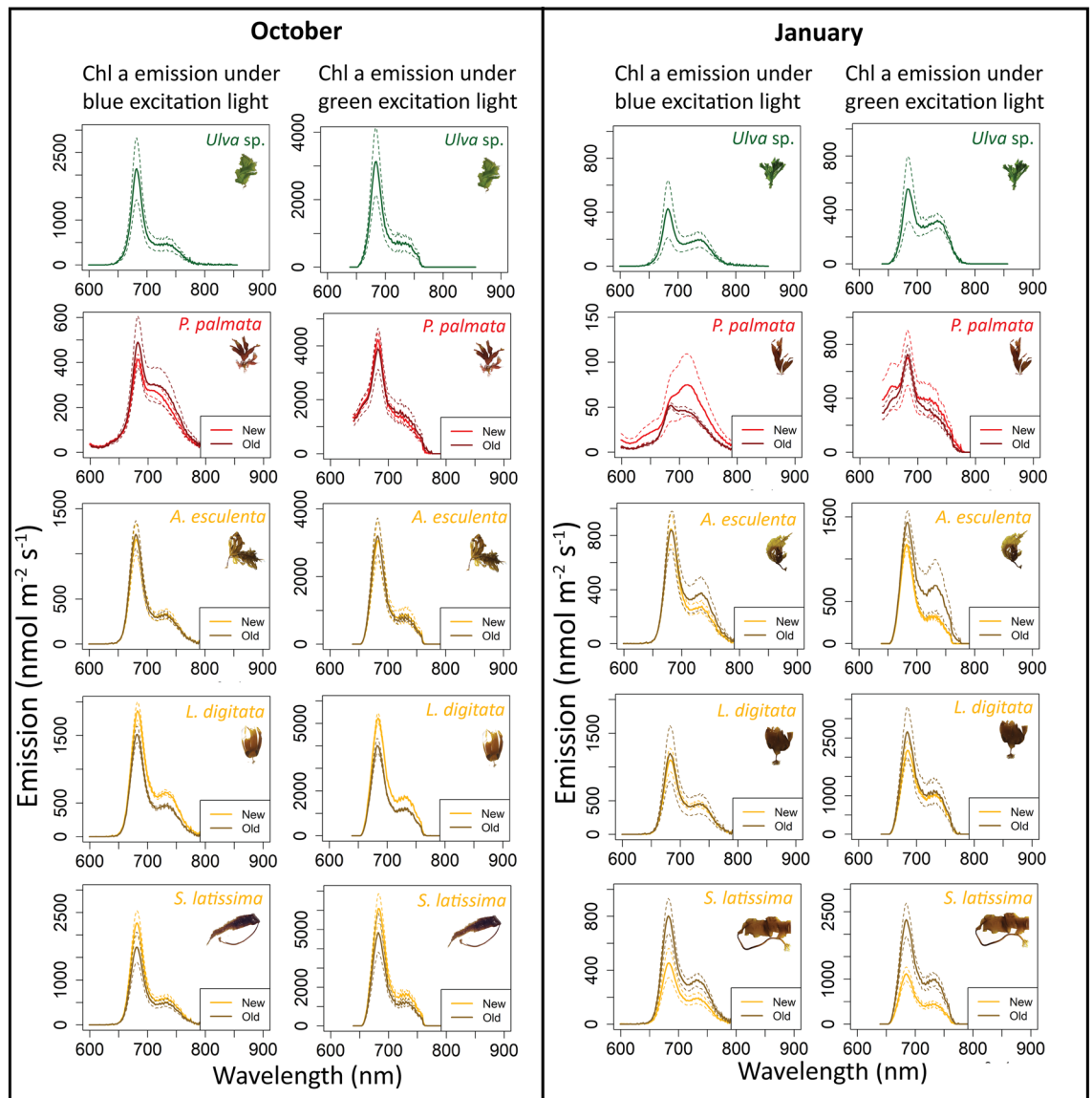


Figure 5. In-vivo Chl a emission spectra from PS II under blue and green excitation light for green, red, and brown algae, measured in October (left) and in January (right). Solid line represents the mean ($n = 3$) and the dotted line is the standard deviation.

emission peak at 685 nm and a corresponding shoulder at 730 nm. Chlorophyll a emission was $\sim 10\times$ higher when exposed to green excitation light relative to blue excitation light (fluorescence emission mean of $\sim 200\text{--}300$ nmol photons $\text{m}^{-2} \text{s}^{-1}$ versus, $\sim 2000\text{--}2500$ nmol photons $\text{m}^{-2} \text{s}^{-1}$) with some variation between new and old tissue.

The total *in-vivo* absorbance of green, red, and brown algae measured in May showed a spectral shift in the Chl a peak which was at 680 nm, 679 nm and 675 nm respectively (Fig. 6c). Similarly, Chl a dip in the reflectance spectra from May was observed at 669 nm for green algae, 677 nm for red algae and 663 nm for brown algae. In January, the Chl a dip in the reflectance curve was observed at 651 nm for green algae, 672 nm for red algae and 664 nm for brown algae (Fig. 6d) which differed from the May measurements (Fig. 6c). No wavelength shifts in the red absorbance peak and corresponding reflectance dip were observed between the triplicates of the same species in May.

Discussion

Our results show that the macroalgae species studied were in better physical state during the Polar Night (in January) than at the end of the light season (in October). Visual evidence for this was the physical appearance of the macroalgal specimens during Polar Night (Fig. 2). In addition, new tissue growth was observed on *P. palmata*, as well as longer lamina in *S. latissima* and *A. esculenta*, providing strong evidence that these species of macroalgae were forming new tissue during the Polar Night. Other species, *Ulva* sp., and *L. digitata*, also grew new tissue during the Polar Night but to a lower extent than *P. palmata*, *A. esculenta*, and *S. latissima*. Dissolved nutrient concentrations (such as nitrate) in Svalbard are high in winter with concentrations of $10\text{--}12 \mu\text{mol L}^{-1}$ ⁹ and close to depleted in summer due to phytoplankton blooms^{2,8,44}. Kelp species are able to store carbohydrates in the form

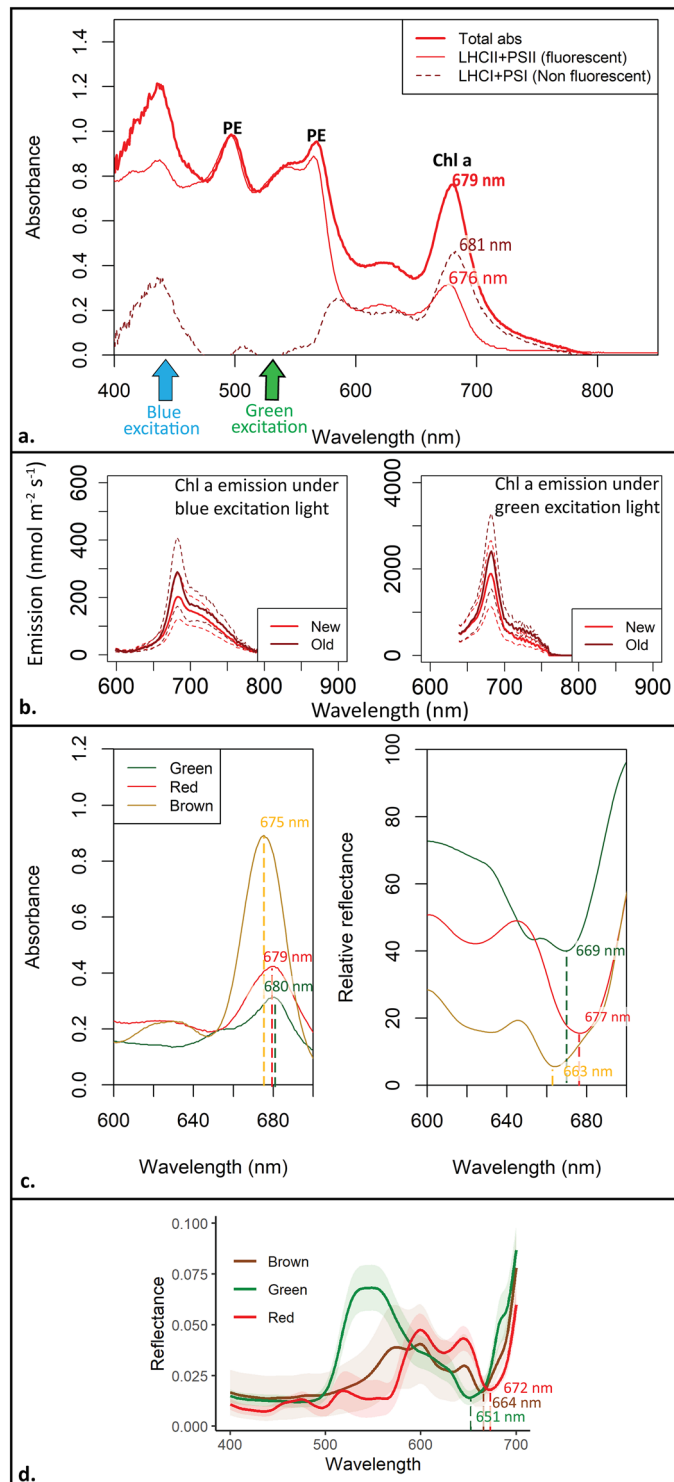


Figure 6. (a) Normalized spectral absorbance measurements for phycobiliprotein-containing red alga *Palmaria palmata*. Thick red solid line: total *in-vivo* pigment absorbance spectra, thin red solid line: absorbance of light harvesting complex II (LHC II) (mainly phycoerythrin, PE) and PS II that provides 95% of Chl a fluorescence signal. Dark red dashed line: Absorbance of light harvesting complex I (LHC I) and PS I (non-fluorescent). The phycobiliprotein peak, dominated by PE, is at 495 nm with a shoulder at 545–560 nm. The Chl a absorbance peaks at 679 nm and 681 nm indicates that the majority of Chl a is bonded to PS I, and the Chl a peak at 676 nm indicates Chl a bonded to PS II, highlighting a spectral shift. Blue and green arrows show the excitation light peaks (452 nm, 525 nm) used for Chl a emission spectra measurements. (b) emission spectra of *P. palmata* under blue (left) and green (right) excitation light. Light red solid line represents new tissue and dark red solid line represents old tissue with the dotted lines representing standard deviation. (c) *In-vivo* spectral absorbance and reflectance of whole tissue of green (*Ulva* sp.), red (*P. palmata*), and brown (*S. latissima*) algae, showing spectral shift of Chl a bonded to PS I or PS II. (d) *In-vivo* reflectance spectra from the Polar Night (January 2020, detailed in Summers et al.²⁶) of green (*Ulva* sp.), red (*P. palmata*) and brown algae (average of *A. esculenta*, *L. digitata*, and *S. latissima*). Light colors indicate the standard error.

of polymer laminarins (also called laminaran, a storage of glucan product of photosynthesis) in their lamina and utilize them to maintain basic physiological functions during winter⁹. However, we suggest that macroalgae during the Polar Night are likely utilizing the available nutrients together with their own carbohydrate storage, not only to maintain photophysiological fitness (discussed below) but to grow new tissue. Growth during the winter (dark season) has been reported in Antarctica, where some red algae species grow new tissue⁸. In contrast, at the end of the light season, the lamina of the kelp species were at their peak state of erosion with seasonal high in epi-growth and the oldest upper parts (~3-year-old tissue) disintegrating in accordance with previous findings during the Polar Night². Meltwater from surrounding glaciers and river-run off peak in July–August⁴⁵ causes a reduction in the underwater light intensity⁴⁶ and disintegration of the kelp lamina.

During the Polar Night, the photosynthetic apparatus of macroalgae studied were functioning as demonstrated by the presented photosynthetic parameters (Fig. 3). Both green algal tissue and new tissue from red algae had lower F_v/F_m in January compared to October. *Palmaria palmata* also had higher E_K in all tissue during the Polar Night. In the kelp species, new tissue in the Polar Night had lower F_v/F_m and higher E_K than at the end of the light season. At the end of the light season, kelp species are acclimated to low light similar to macroalgae living in low light environments. For example, algae living at depth lower than 10m are characterized by an E_K of ~40 $\mu\text{mol photons m}^{-2} \text{ s}^{-1}$ reported in^{47–49}. Thus, high values of E_K here cannot be interpreted as high light acclimation, but as an indicator of a slow working PS II. Similarly, lower F_v/F_m is usually interpreted as a sign of stress as it indicates excess energy dissipation as heat in the antenna complex, resulting in a decreased quantum yield⁵⁰. Our results of lower F_v/F_m during the Polar night, confirm that although the algae are active, they also have a slower functioning PS II. In the case of *S. latissima*, we observed significantly lower F_v/F_m in new tissue versus old tissue at the end of the light season, which could also indicate a separation of function between different sections of the lamina. Such is the case in the large kelp species, *Macrocystis pyrifera* that grows up to 30 m in length, where the tissue close to the meristem capitalizes on nutrients, whereas the apex of the lamina (old tissue) focuses more on photosynthesis^{4,51}.

The light harvesting pigments in the macroalgae studied were non-degraded and functional during both seasons as shown by the shape of the *in-vivo* Chl a emission spectra of PS II characterized by a peak at 685 nm and a corresponding shoulder at 730 nm⁵². Light harvesting pigments play an important role in photophysiology of macroalgae as they capture photons and transfer them to the reaction centers^{17,35,36}. Examining them is important to understand the relationship between the macroalgae and the environment they live in, especially in regards to the quality of light (light intensity and wavelength availability) (21, 43). In green algae, Chl a, Chl b and lutein are the main light-harvesting pigments that absorb blue and red light (Fig. 4). The main light-harvesting pigments in the red algae *P. palmata* are phycobiliproteins (dominated by PE), which absorb light in the blue-green to green part of the spectrum (Fig. 6)² and then funnel the light energy to Chl a in PS II²¹. In brown algae, the main light-harvesting pigments are Chl a, Chl c and fucoxanthin (Fig. 5), where fucoxanthin also absorbs in the blue-green (460–535 nm). In brown algae, fucoxanthin is also the dominating light-harvesting pigment bonded to PS II^{2,43}. In addition to their role in photosynthesis, pigment composition determines which wavelengths of light available can be harvested. As mentioned above, water clarity varies between seasons, with phytoplankton blooms in spring and highest sedimentation from melt water and river run-off in July–August⁹. Thus, even though light availability in air is high from May to October, the corresponding underwater light availability can be highly reduced due to phytoplankton, suspended matter, and colored dissolved organic matter.

We observed that *Ulva* sp. and *P. palmata* accumulated pigments during the Polar Night. Pigment accumulation under low light conditions (such as under ice) were found to be correlated with an increase in maximum photosynthetic rates in green, red, and brown algae from Kongsfjorden⁵³, indicating that the algae were acclimating to decreasing light. In contrast, in kelp species, we observed stable pigment concentrations between seasons. Thus, they were not acclimating to the light conditions of the Polar Night by regulating pigment concentrations. Therefore, the reduced photosynthetic activity must be due to PS II not being fully active in the kelp species examined. We hypothesize that there may be a shortage or a slow turnover of the D1 protein during the Polar Night. The polypeptide D1 is crucial to the electron transfer as they bind Chl a for optimal photosynthesis⁵⁴. However, the synthesis of the D1 protein is activated by light at a given pH optimum and the absorbed quanta is dependent on a functional photosynthetic unit comprising of LHC II, LHC I, PS II, and PS I⁵⁵. The D1 protein synthesis and activation during the Polar Night and as light becomes available may be a major component to be studied in the future.

The pigment distribution between PS I and PS II is an important factor altering the Chl a emission spectra. The corresponding *in-vivo* absorbance and a_{PSII} in *P. palmata* enable us to determine the fraction of Chl a in PS I and II. We use *P. palmata* in May as a case study to illustrate how the absorbance spectra helped us interpret the emission spectra (Figs. 5 and 6). Measurements from *P. palmata* show that, the emission of Chl a in PS II under green excitation light was 8 to 10 × higher than under blue excitation light where Chl a in PS I is excited (Fig. 6b), in accordance with Grzymiski et al.⁴³. When adjusting for differences in the excitation light intensity settings of PAM-spectrometer, the signal from the green emission needs to be decreased by 33% more than what is shown in Figs. 5 and 6b to provide the same energy output in blue and green. If this is adjusted for, the emission of Chl a in PS II was 3 × higher (in May) under green excitation light than under the blue excitation light. We suggest that the difference in the intensity of the emission spectra under green (PS II) and blue (PS I) excitation light is an indication of differences in light energy transfer to PS II relative to PS I with 30% of Chl a in PS II and the rest in PS I. This is comparable to the results of using the spectral absorbance.

By using a_{PSII} , outlined in Fig. 6a, we calculated the fraction of Chl a bonded to PS II. The Chl a peak at 676 nm a_{PSII} was ~40% of the Chl a peak at 679 nm of the *in-vivo* total absorbance. We, therefore, conclude that ~40% of Chl a in *P. palmata* is bonded to PS II with most of the Chl a (60%) bonded to PS I. This is in accordance with both Grzymiski et al.⁴³ and Johnsen and Sakshaug³⁹. We, thus, observed a slight difference in estimated [Chl a] in PS II of 10% between the interpreted *in-vivo* Chl a emission spectra and the a_{PSII} calculated fraction (Fig. 6).

Our Chl a emission data for green, red, and brown macroalgae indicate that there are variations between species, tissue age, and seasonality (Fig. 5). However, further investigation with different intensity settings of the spectrometer excitation light is needed to align the emission spectra interpretation with the a_{PSII} results. Calculating the fraction of Chl a in PS II vs PS I is necessary to accurately calculate O_2 production from PAM fluorescence measurements³⁷. A factor of 0.5 or 0.6 (50 and 60% of Chlorophyll a in PS II) is usually used by default to calculate the theoretical fraction of quanta absorbed^{37,39,52}. This is the first study, to our knowledge, using the mini spectrometer of the Diving PAM II to compare Chl a emission spectra between species and seasons, additional challenges to the interpretation may be caused by the package effect (intracellular self-shading) that includes differences in the tissue thickness, pigment concentration in the chloroplasts, density of chloroplast and non-photochemical quenching⁴³. More research looking at the Chl a emission spectra from different pigment groups of algae, grown under different environmental conditions, and with different intensity and integration time settings of Chl a emission spectrometer, is needed to investigate the package effect as well as to validate our interpretations and assumptions.

We observed a spectral shift of 3 nm in the *in-vivo* absorbance peak of Chl a relative to the a_{PSII} in the red absorption peak region. The Chl a absorbance peak was at 679 nm for the total absorbance, at 676 nm for a_{PSII} , and at 681 nm indicating that the majority of Chl a is attached to PS I. This difference spectrum is in accordance with our findings discussed above (Fig. 6a). The observed spectral shift is due to Chl a being bonded to different proteins in PS I, PS II and their corresponding light-harvesting complexes (LHC I and II)^{38,39}. With most of the Chl a in *P. palmata* bonded to PS I, the fluorescence emission detected by the Diving PAM II was low both for PS II kinetics (fluorescence yield measurements) and corresponding *in-vivo* Chl a emission spectra.

We also observed a spectral shift in the *in-vivo* Chl a (644–680 nm), Chl b (650 nm), and Chl c (600 and 630 nm) peaks in the absorbance and corresponding reflectance spectra of green, red, and brown algae indicating the fraction of Chl a bonded to PS II and PS I as well as their corresponding light-harvesting complexes (Fig. 6b,c). The *in-vivo* Chl a red absorbance maximum peak in brown algae (*S. latissima*) was at 675 nm, indicating that most of the Chl a is bonded to PS II. In contrast, green (*Ulva* sp.) and red (*P. palmata*) algae have the *in-vivo* Chl a absorbance peak at 680 nm and 679 nm, respectively, indicating that the majority of Chl a is bonded to PS I in accordance with our interpretation of the emission spectra detailed above. These results are in accordance with phytoplankton classes of chromophytes (Chl c containing phytoplankton classes), Chl b containing phytoplankton (chlorophytes, euglenophytes, and prasinophytes), and phycobiliprotein containing cryptophytes and cyanobacteria, outlined in Johnsen and Sakshaug³⁹. Similarly, we observed a shift in the *in-vivo* spectral reflectance dips in the red part of the spectrum. The reflectance dip in green algae was lower at 651 nm in January and 669 nm in May probably caused by the relatively high absorbance of Chl b (650 nm) and Chl a attached to PS I (679–680)⁴³. In contrast, the *in-vivo* reflectance dip in red algae was at 672 nm in January and at 677 nm in May. The seasonal spectral reflectance shift may be due to varying ratio of Chl a in PS I and PS II between seasons. The brown algae have a similar reflectance dip in January and May at 664 nm and 663 nm respectively, partly due to absorbance impact of Chl c (peak at 630 nm).

Pigment composition and concentration is also important for interpretation of *in-situ* monitoring using UHI as they determine the spectral reflectance signature of macroalgae [outlined in 26]. For example, Chl a has been widely used to determine phytoplankton biomass⁵⁶. With UHI mapping, pigment composition, allows us to differentiate between pigment groups (green, red, and brown algae)²⁶. This study provides additional information regarding the health state in terms of photophysiological and physical state of the species present. In conclusion, we show that the examined macroalgae were growing new tissue during the Polar Night that they are photophysiologicaly functioning. High E_K and low F_v/F_m in kelp species indicate a PS II with slower activity during the Polar Night relative to the end of the light season. We also demonstrate how the *in-vivo* Chl a emission spectra, which reflect the light energy transferred to PS II in all species, could be interpreted. The *in-vivo* absorbance spectra were used to interpret the *in-vivo* Chl a emission spectra to determine the ratio of [Chl a] in PS I vs PS II. We acknowledge that more research and experimentation is needed to further investigate reported seasonal variation in emission intensity. We also measured a spectral shift in the *in-vivo* Chl a absorbance and reflectance peaks in the red part of the visible spectrum, giving us additional confirmation about whether the Chl a are bonded to PS I or PS II. This study provides evidence of tissue growth and indication of photophysiological activity in red, green, and brown macroalgae during the Polar Night, complementing biodiversity and areal cover information gathered through ROV-UHI mapping of kelp forest habitat at the same site and time as this study²⁶. Combining photophysiology and health state with UHI habitat mapping also provides an overview of the study site at different time and spatial scales which may be important in future identification, mapping and monitoring of underwater habitats.

Data availability

Light data are available through open access through NIRD (National Infrastructure for Research Data). The data are published in datasets covering annual time series (2020) from spectroradiometer (raw data and E_{PAR} data): Berge, J., et al. USSIMO Spectroradiometer Raw Data Time Series (2020) Measured under the Dome of a Light Observatory in the Arctic (Ny-Ålesund, Svalbard, Norway) [Data Set], (Norstore, 2021). Data from the all-sky camera can be found: Johnsen, G., et al. Pictures from an All-Sky Camera with Hourly Resolution from the Light Observatory at Ny-Ålesund, Svalbard, Norway (Complete Year 2020) [Data Set], (Norstore, 2021). Other datasets generated and analyzed during the current study are available from the corresponding author on reasonable request.

Received: 27 June 2023; Accepted: 3 October 2023

Published online: 20 October 2023

References

- Berge, J. *et al.* Unexpected levels of biological activity during the polar night offer new perspectives on a warming arctic. *Curr. Biol.* **25**, 2555–2561. <https://doi.org/10.1016/j.cub.2015.08.024> (2015).
- Johnsen, G., Leu, E. & Gradinger, R. Marine micro- and macroalgae in the Polar Night in *Polar Night Marine Ecology Advances in Polar Ecology* Vol. 4 (ed. Berge, J., Johnsen, G., Cohen, J.) Ch. 4, 67–112 (Springer, 2020).
- Lüning, K. & tom Dieck, I. Environmental triggers in algal seasonality. *Botanica Marina* **32**, 389–398, doi:<https://doi.org/10.1515/botm.1989.32.5.389> (1989).
- Raven, J. A. & Hurd, C. L. Ecophysiology of photosynthesis in macroalgae. *Photosynth. Res.* **113**, 105–125. <https://doi.org/10.1007/s11120-012-9768-z> (2012).
- Wang, Y. *et al.* A comparative study of the photosynthetic capacity in two green tide macroalgae using chlorophyll fluorescence. *Springer Plus* **5**, doi:<https://doi.org/10.1186/s40064-016-2488-7> (2016).
- Berge, J., Johnsen, G., & Cohen, J. H. (eds.). *Polar Night Marine Ecology* Vol. 4 (Springer, 2020). <https://doi.org/10.1007/978-3-030-33208-2>
- Johnsen, G. *et al.* All-sky camera system providing high temporal resolution annual time series of irradiance in the Arctic. *Appl. Opt.* **60**, 6456–6456. <https://doi.org/10.1364/ao.424871> (2021).
- Wiencke, C. *et al.* Life strategy, ecophysiology and ecology of seaweeds in polar waters. *Rev. Environ. Sci. Biotechnol.* **6**, 95–126. <https://doi.org/10.1007/s11157-006-9106-z> (2007).
- Scheschonk, L. *et al.* Arctic kelp eco-physiology during the polar night in the face of global warming: A crucial role for laminarin. *Mar. Ecol. Prog. Ser.* **611**, 59–74. <https://doi.org/10.3354/meps12860> (2019).
- Dunton, K. H. & Schell, D. M. Seasonal carbon budget and growth of *Laminaria solidungula* in the Alaskan High Arctic. *Mar. Ecol. Prog. Ser.* **31**, 57–66 (1986).
- Dunton, K. H. Growth and production in *Laminaria solidungula*: relation to continuous underwater light levels in the Alaskan High Arctic. *Mar. Biol.* **106**, 297–304. <https://doi.org/10.1007/BF01314813> (1990).
- Belseth, E. *Eco-physiology of the Arctic kelp Laminaria solidungula-using divers, Remotely Operated Vehicle and Pulse Amplitude Modulated fluorometry* Msc thesis, Norwegian University of Science and Technology, (2012).
- Dunton, K. H. Growth of dark-exposed *Laminaria saccharina* (L.) Lamour. and *Laminaria solidungula* J. Ag. (laminariales: phaeophyta) in the Alaskan Beaufort Sea. *J. Exp. Mar. Biol. Ecol.* **94**, 181–189. [https://doi.org/10.1016/0022-0981\(85\)90057-7](https://doi.org/10.1016/0022-0981(85)90057-7) (1985).
- Bartsch, I. *et al.* The genus *Laminaria* sensu lato: Recent insights and developments. *Eur. J. Phycol.* **43**, 1–86. <https://doi.org/10.1080/09670260701711376> (2008).
- Cohen, J. H., Berge, J., Moline, M. A., Johnsen, G. & Zolich, A. P. Light in the Polar Night in *Polar Night Marine Ecology: Life and Light in the Dead of Night* Vol. 4 (eds Jørgen Berge, Geir Johnsen, & Jonathan H. Cohen) Ch. 3, 37–66 (Springer, 2020).
- Berge, J. *et al.* Artificial light during the polar night disrupts Arctic fish and zooplankton behaviour down to 200 m depth. *Commun. Biol.* **3**, 102. <https://doi.org/10.1038/s42003-020-0807-6> (2020).
- Hanelt, D., Wiencke, C. & Bischof, K. Photosynthesis in Marine Macroalgae in *Photosynthesis in Algae. Advances in Photosynthesis and Respiration* Vol. 14 (eds A. W. D. Larkum, S. E. Douglas, & J. A. Raven) 413–435 (Springer, 2003).
- Fredriksen, S. *et al.* Biodiversity of benthic macro- and microalgae from svalbard with special focus on Kongsfjorden in *The Ecosystem of Kongsfjorden, Svalbard* Vol. 2 (eds Haakon Hop & Christian Wiencke) 331–371 (Springer International Publishing, 2019).
- Sakshaug, E. *et al.* Parameters of photosynthesis: definitions, theory and interpretation of results. *J. Plankton Res.* **19**, 1637–1670. <https://doi.org/10.1093/plankt/19.11.1637> (1997).
- Schreiber, U. Pulse-Amplitude-Modulation (PAM) Fluorometry and Saturation Pulse Method: An Overview in *Chlorophyll a Fluorescence: A Signature of Photosynthesis* Vol. 19 (eds George Christos Papageorgiou & Govindjee) 279–319 (Springer, 2004).
- Rowan, K. S. *Photosynthetic pigments of algae* (Cambridge University Press, 1989).
- Valle, K. C. *et al.* System responses to equal doses of photosynthetically usable radiation of blue, green, and red light in the marine Diatom *Phaeodactylum tricoratum*. *PLOS ONE* **9**, e114211. <https://doi.org/10.1371/journal.pone.0114211> (2014).
- Konik, M., Darecki, M., Pavlov, A. K., Sagan, S. & Kowalczyk, P. Darkening of the Svalbard Fjords waters observed with satellite ocean color imagery in 1997–2019. *Front. Mar. Sci.* <https://doi.org/10.3389/fmars.2021.699318> (2021).
- Niedzwiedz, S. & Bischof, K. Glacial retreat and rising temperatures are limiting the expansion of temperate kelp species in the future Arctic. *Limnol. Oceanogr.* **68**, 816–830. <https://doi.org/10.1002/lno.12312> (2023).
- Volent, Z., Johnsen, G. & Sigernes, F. Kelp forest mapping by use of airborne hyperspectral imager. *J. Appl. Remote Sens.* **1**, 011503–011503. <https://doi.org/10.1117/1.2822611> (2007).
- Summers, N. *et al.* Underwater Hyperspectral Imaging of Arctic Macroalgal Habitats during the Polar Night Using a Novel Mini-ROV-UHI Portable System. *Remote Sens.* **14** (2022).
- Dankworth, M., Heinrich, S., Fredriksen, S. & Bartsch, I. DNA barcoding and mucilage ducts in the stipe reveal the presence of *Hedophyllum nigripes* (Laminariales, Phaeophyceae) in Kongsfjorden (Spitsbergen). *J. Phycol.* **56**, 1245–1254. <https://doi.org/10.1111/jpy.13012> (2020).
- Borum, J., Pedersen, M., Krause-Jensen, D., Christensen, P. & Nielsen, K. Biomass, photosynthesis and growth of *Laminaria saccharina* in a high-arctic fjord, NE Greenkand. *Mar. Biol.* **141**, 11–19. <https://doi.org/10.1007/s00227-002-0806-9> (2002).
- Ralph, P. J. & Gademann, R. Rapid light curves: A powerful tool to assess photosynthetic activity. *Aquat. Bot.* **82**, 222–237. <https://doi.org/10.1016/j.aquabot.2005.02.006> (2005).
- Hancke, T. B., Hancke, K., Johnsen, G. & Sakshaug, E. Rate of O₂ production derived from pulse-amplitude-modulated fluorescence: testing three biooptical approaches against measured O₂-production rate. *J. Phycol.* **44**, 803–813. <https://doi.org/10.1111/j.1529-8817.2008.00509.x> (2008).
- Genty, B., Briantais, J. M. & Baker, N. R. The relationship between the quantum yield of photosynthetic electron transport and quenching of chlorophyll fluorescence. *Biochim. Biophys. Acta Gen. Subjects* **990**, 87–92. [https://doi.org/10.1016/S0304-4165\(89\)80016-9](https://doi.org/10.1016/S0304-4165(89)80016-9) (1989).
- R Core Team. R: A language and environment for statistical computing. R Foundation for Statistical Computing, Vienna, Austria. URL <https://www.R-project.org/> (2021).
- Silsbe, G. M. & Malkin, S. Y. Phytotools: Phytoplankton Production Tools, An R package available on CRAN: <https://cran.r-project.org/web/packages/phytotools/index.html>. 2015
- Revell, L. J. Phytotools: A R package for phylogenetic comparative biology (and other things). *Methods Ecol. Evol.* **3**, 217–223. <https://doi.org/10.1111/j.2041-210X.2011.00169.x> (2012).
- Clayton, R. K. The biophysical problems of photosynthesis. *Science* **149**, 1346–1354 (1965).
- Mirkovic, T. *et al.* Light absorption and energy transfer in the antenna complexes of photosynthetic organisms. *Chem. Rev.* **117**, 249–293. <https://doi.org/10.1021/acs.chemrev.6b00002> (2017).
- Butler, W. L. Energy distribution in the photochemical apparatus of photosynthesis. *Annu. Rev. Plant Physiol.* **29**, 345–378. <https://doi.org/10.1146/annurev.pp.29.060178.002021> (1978).
- Johnsen, G., Prézélin, B. B. & Jovine, R. V. M. Fluorescence excitation spectra and light utilization in two red tide dinoflagellates. *Limnol. Oceanogr.* **42**, 1166–1177. https://doi.org/10.4319/lo.1997.42.5_part_2.1166 (1997).

39. Johnsen, G. & Sakshaug, E. Biooptical characteristics of PSII and PSI in 33 species (13 pigment groups) of marine phytoplankton, and the relevance for pulse amplitude-modulated and fast-repetition-rate fluorometry. *J. Phycol.* **43**, 1236–1251. <https://doi.org/10.1111/j.1529-8817.2007.00422.x> (2007).
40. Walz, H. *Underwater Fluorometer Diving-Pam, Submersible Photosynthesis Yield Analyzer, Handbook of Operation*. (Heinz Walz GmbH, 2020)
41. Rodríguez, F. *et al.* Photoacclimation in phytoplankton: implications for biomass estimates, pigment functionality and chemotaxonomy. *Mar. Biol.* **148**, 963–971. <https://doi.org/10.1007/s00227-005-0138-7> (2006).
42. Roy, S. *et al.* (eds) *Phytoplankton Pigments: Updates on Characterization, Chemotaxonomy and Applications in Oceanography* (Cambridge University Press, 2011).
43. Grzymalski, J., Johnsen, G. & Sakshaug, E. The significance of intracellular self-shading on the biooptical properties of brown, red, and green macroalgae. *J. Phycol.* **33**, 408–414. <https://doi.org/10.1111/j.0022-3646.1997.00408.x> (1997).
44. Piquet, A. M. T. *et al.* Springtime phytoplankton dynamics in Arctic Krossfjorden and Kongsfjorden (Spitsbergen) as a function of glacier proximity. *Biogeosciences* **11**, 2263–2279. <https://doi.org/10.5194/bg-11-2263-2014> (2014).
45. Tverberg, V. *et al.* The Kongsfjorden transect: Seasonal and inter-annual variability in hydrography in *The Ecosystem of Kongsfjorden, Svalbard* (eds Haakon Hop & Christian Wiencke) 49–104 (Springer International Publishing, 2019).
46. Pavlov, A. K. *et al.* The underwater light climate in Kongsfjorden and its ecological implications in *The Ecosystem of Kongsfjorden, Svalbard* (eds Haakon Hop & Christian Wiencke) 137–170 (Springer International Publishing, 2019).
47. Kirst, G. O. & Wiencke, C. Ecophysiology of polar algae. *Journal of Phycology* **31**, 181–199. <https://doi.org/10.1111/j.0022-3646.1995.00181.x> (1995).
48. Weykam, G. & Wiencke, C. Seasonal photosynthetic performance of the endemic Antarctic red alga *Palmaria decipiens* (Reinsch) Ricker. *Polar Biol.* **16**, 357–361. <https://doi.org/10.1007/BF02342184> (1996).
49. Gómez, I., Weykam, G., Klöser, H. & Wiencke, C. Photosynthetic light requirements, metabolic carbon balance and zonation of sublittoral macroalgae from King George Island (Antarctica). *Mar. Ecol. Prog. Ser.* **148**, 281–293 (1997).
50. Krause, G. H. & Weis, E. Chlorophyll fluorescence and photosynthesis: the basics. *Annu. Rev. Plant Physiol. Plant Mol. Biol.* **42**, 313–349. <https://doi.org/10.1146/annurev.pp.42.060191.001525> (1991).
51. Raven, J. A. Long-distance transport in non-vascular plants. *Plant Cell Environ.* **26**, 73–85. <https://doi.org/10.1046/j.1365-3040.2003.00920.x> (2003).
52. Suggett, D. J. *et al.* (eds) *Aquatic Sciences: Methods and Applications* (Springer, 2010).
53. Aguilera, J., Bischof, K., Karsten, U., Hanelt, D. & Wiencke, C. Seasonal variation in ecophysiological patterns in macroalgae from an Arctic fjord. II. Pigment accumulation and biochemical defence systems against high light stress. *Mar. Biol.* **140**, 1087–1095. <https://doi.org/10.1007/s00227-002-0792-y> (2002).
54. Larkum, A. W. D. *et al.* (eds) *Photosynthesis in Algae* (Springer, 2003).
55. Inagaki, N. Processing of D1 protein: A mysterious process carried out in thylakoid lumen. *Int. J. Mol. Sci.* **23**, 2520 (2022).
56. Johnsen, G. *et al.* Optical monitoring of phytoplankton bloom pigment signatures in *Phytoplankton Pigments* (eds S. Roy, C. Llewellyn, E. Egeland, & G. Johnsen) Chap 14, pp. 538–606 (Cambridge: Cambridge University Press, 2011).

Acknowledgements

We would like to thank Aksel Mogstad and Håvard Løvås for help during field work during the Polar Night (January 2020) and Andrea Faltynkova (October 2020). This project was financed by the Norwegian Research Council (NRC): Nansen Legacy (NRC 276730), Arctic ABC-D infrastructure with ArcLight observatory (NRC 245923), Deep Impact (NRC 300333), Center of Excellence AMOS (NRC 223254), MoniTare (NRC 315514) and Identification and mapping of marine microplastics and macroalgae (NRC 318210). We would also like to thank the students and teachers at UNIS (University Centre in Svalbard) course AB323 “Light and primary production in the Arctic” during the May 2022 campaign.

Author contributions

NS and GJ conducted the field work (acquiring data), NS did the formal analysis and the original draft, all authors contributed to the interpretation of the data, review and editing of the manuscript. GJ and GF were responsible for supervision.

Funding

Open access funding provided by Norwegian University of Science and Technology.

Competing interests

The authors declare no competing interests.

Additional information

Correspondence and requests for materials should be addressed to N.S.

Reprints and permissions information is available at www.nature.com/reprints.

Publisher’s note Springer Nature remains neutral with regard to jurisdictional claims in published maps and institutional affiliations.



Open Access This article is licensed under a Creative Commons Attribution 4.0 International License, which permits use, sharing, adaptation, distribution and reproduction in any medium or format, as long as you give appropriate credit to the original author(s) and the source, provide a link to the Creative Commons licence, and indicate if changes were made. The images or other third party material in this article are included in the article’s Creative Commons licence, unless indicated otherwise in a credit line to the material. If material is not included in the article’s Creative Commons licence and your intended use is not permitted by statutory regulation or exceeds the permitted use, you will need to obtain permission directly from the copyright holder. To view a copy of this licence, visit <http://creativecommons.org/licenses/by/4.0/>.

© The Author(s) 2023